Collider Physics at e^+e^- Colliders

To begin these lectures, I will review some aspects of the interaction of massless fermions and vector bosons. At the energies of the LHC, it is a good approximation to ignore all quark masses except for that of the top quark. It will be good to establish some notation to describe massless fermions.

You all know that a spin-1/2 particle is described by the Dirac equation

$$(i\gamma \cdot \partial - m)\Psi = 0$$

I will use the basis for γ^μ matrices

$$\gamma^\mu = \begin{pmatrix} 0 & \sigma^\mu \\ \bar{\sigma}^\mu & 0 \end{pmatrix}$$

$$\sigma^\mu = (1, \vec{\sigma})^\mu \qquad \bar{\sigma}^\mu = (1, -\vec{\sigma})^\mu$$

If we ignore the mass term, this equation splits into two 2-component equations

$$\Psi = \begin{pmatrix} \psi_L \\ \psi_R \end{pmatrix}$$

$$i\bar{\sigma} \cdot \partial \psi_L = 0 \qquad\qquad i\sigma \cdot \partial \psi_R = 0$$

The two equations are related by the fact that, if ψ_L satisfies the first equation, then

$$\psi_R = i\sigma^2 \psi_L^* = \varepsilon \psi_L^* \qquad \varepsilon = \begin{pmatrix} 0 & 1 \\ -1 & 0 \end{pmatrix}$$

satisfies the second.

We can write explicit solutions to these equation that we can then use throughout the course. Begin with the equation for the left-handed fermion field ψ_L. These have the form

$$\psi_L(x) = u_L(p) e^{-ip \cdot x}$$

where $p^2 = 0$ and $u_L(p)$ is a 2-component spinor. For $\vec{p} \parallel \hat{3}$,

$$\hat{p} = (p \; 0 \; 0 \; p)^{\mu}$$

the ψ_L equation becomes

$$p \cdot \bar{\sigma} \; u_L(p) = 0$$

$$[p + \vec{p} \cdot \vec{\sigma}] \; u_L(p) = 0$$

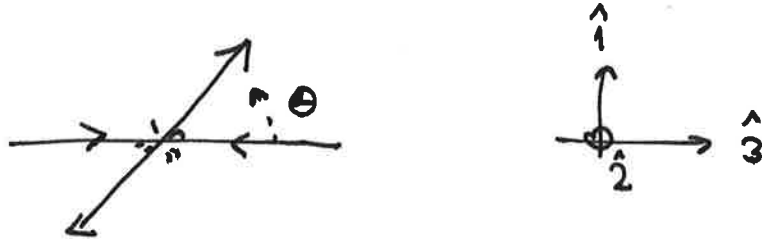or

$$p [1 + \sigma^3] \; u_L(p) = 0$$

Then

$$u_L(p) = \sqrt{2p} \begin{pmatrix} 0 \\ 1 \end{pmatrix}$$

The spinors are normalized to

$$u^{\dagger} u = 2p^0$$

2

and the spin orientation is left-handed with respect to $\hat{3}$, as we should expect. The form of the spinor for a general direction of $\vec{p}$ is found by rotating this solution. I will always try where it is possible to set up a 2-body scattering process in the $hat3$-$\hat{1}$ plane,

Then

$$u_L(p) = \sqrt{2p} \begin{pmatrix} -\sin\Theta/2 \\ \cos\Theta/2 \end{pmatrix}$$

The antiparticle of a left-handed fermion is a right-handed antifermion. This corresponds to a solution to the Weyl equation

$$\psi_L(x) = v_R(p)\, e^{+ip\cdot x}$$

The spinor $v_R(p)$ obeys

$$p\cdot\bar{\sigma}\; v_R(p) = 0$$

and this is the same equation, with the same solutions, as before. It is straightforward to derive the complementary results for right-handed fermions and left-handed antifermions.

Then, we have the set of 2-component spinors

$$f_L \qquad u_L = \sqrt{2p} \begin{pmatrix} -\sin\theta_h \\ \cos\theta_h \end{pmatrix} \qquad \bar{f}_R: \quad v_R = \sqrt{2p} \begin{pmatrix} -\sin\theta_h \\ \cos\theta_h \end{pmatrix}$$

$$f_R \qquad u_R = \sqrt{2p} \begin{pmatrix} \cos\theta_h \\ \sin\theta_h \end{pmatrix} \qquad \bar{f}_L: \quad v_L = \sqrt{2p} \begin{pmatrix} \cos\theta_h \\ \sin\theta_h \end{pmatrix}$$

It is very convenient to also record the spinors for particles moving in the opposite direction

$$f_L \qquad u_L = \sqrt{2p} \begin{pmatrix} -\cos\theta_h \\ -\sin\theta_h \end{pmatrix} = v_R \qquad \bar{f}_R$$

$$f_R \qquad u_R = \sqrt{2p} \begin{pmatrix} -\sin\theta_h \\ \cos\theta_h \end{pmatrix} = v_L \qquad \bar{f}_L$$

The spinors we have derived here play the same role in calculation as the polarization vectors for vector particles. For vectors, it is more obvious what the appropriate vectors should be. In the rest frame of a massive vector particle, there are 3 distinct polarization vectors corresponding to right-handed, zero, and left-handed spin about the $\hat{3}$ axis,

$$\varepsilon^\mu(p) = \begin{cases} \frac{1}{\sqrt{2}}(0 \; 1 \; i \; 0)^\wedge & R \\ (0 \; 0 \; 0 \; 1)^\wedge & O \\ \frac{1}{\sqrt{2}}(0 \; 1 \; -i \; 0)^\wedge & L \end{cases}$$

Boosting these vectors in the $\hat{3}$ direction gives

$$\varepsilon^\mu(p) = \begin{cases} \frac{1}{\sqrt{2}}(0 \; 1 \; i \; 0)^\wedge & R \\ (P/m \; , \; 0 \; , \; 0 \; , \; E/m)^\wedge & O \\ \frac{1}{\sqrt{2}}(0 \; 1 \; -i \; 0)^\wedge & L \end{cases}$$

It is apparent that something goes wrong with the 0 polarization states as $m \to 0$ or $E \to \infty$. Fortunately, for massless vector bosons, the 0 polarization state does not

exist. Only the R and L states are produced as physical states by gauge-invariant interactions. For massive vector bosons, the polarization state 0 must exist, and we will eventually need to understand its properties. I will discuss this set of questions in lecture 5 of this series.
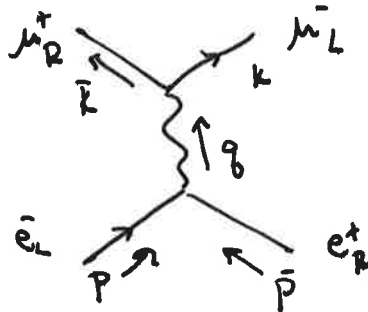
The R and L polarization vectors rotated to an angle θ in the $\hat{3}$-$\hat{1}$ plane are

$$\epsilon^{\mu}(q) = \begin{cases} \frac{1}{\sqrt{2}}(0, \cos\theta, i, -\sin\theta)^{\sim} & R \\ \frac{1}{\sqrt{2}}(0, \cos\theta, i, -\sin\theta)^{\sim} & L \end{cases}$$

and those rotated to the opposite direction are

$$\epsilon^{\mu}(q) = \begin{cases} \frac{1}{\sqrt{2}}(0, -\cos\theta, i, \sin\theta)^{\wedge} \\ \frac{1}{\sqrt{2}}(0, -\cos\theta, -i, \sin\theta)^{\wedge} \end{cases}$$

I will now make some use of these formulae by recalling the properties of the simplest QED process, $e^{+}e^{-} \rightarrow \mu^{+}\mu^{-}$. For definiteness, consider the state with definite spins $e_{L}^{-}e_{R}^{+} \rightarrow \mu_{L}^{-}\mu_{R}^{+}$.

The matrix element for this scattering process is

$$i\mathcal{M} = (-ie)^{2} \, u^{\dagger}(k)\bar{\sigma}^{\mu}v(\bar{k}) \, \frac{-i}{q^{2}} \, v^{\dagger}(\bar{p})\bar{\sigma}_{\mu}u(p)$$

Setting $\vec{p} \parallel 3$, we can compute

5

$$v^\dagger(p)\,\bar\sigma^\mu\, u(p) = (\sqrt{2}p)^2\,(-1\ 0)\,(1,-\vec\sigma^*)\binom{0}{1}$$

$$= 2p\,(0\ 1\ -i\ 0)^\mu$$

This is exactly the left-handed polarization vector for the intermediate virtual photon, as we might have expected from angular momentum conservation

For an initial state at an angle with respect to the $\hat 3$ axis,

$$v^\dagger(p)\,\bar\sigma^\mu\, u(p) = 2p\,\left(-\cos\tfrac{\theta}{2},\ \sin\tfrac{\theta}{2}\right)(1,-\vec\sigma)^\mu\begin{pmatrix}-\sin\tfrac{\theta}{2}\\ \cos\tfrac{\theta}{2}\end{pmatrix}$$

$$= 2p\,\left(0,\ \cos^2\tfrac{\theta}{2}-\sin^2\tfrac{\theta}{2},\ -i\left(\cos^2\tfrac{\theta}{2}+\sin^2\tfrac{\theta}{2}\right),\ -2\sin\tfrac{\theta}{2}\cos\tfrac{\theta}{2}\right)$$

we have

$$v^\dagger(p)\,\bar\sigma^\mu\, u(p) = 2p\,(1\ \cos\theta,\ -i,\ -\sin\theta)^\mu$$

which is just the appropriate rotation of this vector. We now recognize

$$v_R^\dagger(p)\,\bar\sigma^\mu\, u_L(p) = 2\sqrt{2}\,p\,\,\varepsilon_L^\mu(p)$$

and, similarly, you can show

$$v_L^\dagger(\bar{p})\, \bar{\sigma}^\mu\, u_R(p) = 2\sqrt{2}\; \varepsilon_R^\mu(p)$$

We can use these results in two ways. First, we can use the find the angular dependence of the annihilation reaction $e_L^- e_R^+ \to \mu_L^- \mu_R^+$. The matrix element above becomes

$$\mathcal{M} = \frac{ie^2}{q^2}\; 2\cdot(2p)^2\; \varepsilon_L^{+\mu}(k)\, \Sigma_L(p)$$

$$= \frac{ie^2}{q^2}\, 2q^2\; \tfrac{1}{2}\,(1\;\cos\theta,\; i\,-\sin\theta)\cdot(0\;\;1\;\;-i\;\;0)$$

$$= ie^2\,(1+\cos\theta)$$

From this we find

$$\frac{d\sigma}{d\cos\theta}\,(e_L^- e_R^+ \to \mu_L^- \mu_R^+) = \frac{\pi\alpha^2}{2s}\,(1+\cos\theta)^2 = \frac{d\sigma}{d\cos\theta}\,(e_R^- e_L^+ \to \mu_R^- \mu_L^+)$$
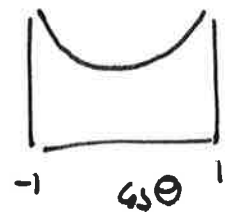
and, similarly,

$$\frac{d\sigma}{d\cos\theta}\,(e_L^- e_R^+ \to \mu_R^- \mu_L^+) = \frac{\pi\alpha^2}{2s}\,(1-\cos\theta)^2 = \frac{d\sigma}{d\cos\theta}\,(e_R^- e_L^+ \to \mu_L^- \mu_R^+)$$
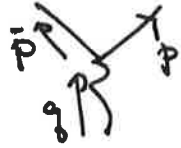
These equations give the familiar canonical results for $e^+ e^-$ annihilation

$$\frac{d\sigma}{d\cos\theta}\Big|_{\text{pol sm + avg}} = \frac{\pi\alpha^2}{2s}\,(1+\cos^2\theta)$$

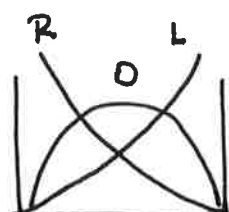$$\sigma_T(e^+ e^- \to \mu^+ \mu^-) = \frac{4\pi\alpha^2}{3s}$$

7

Another use of these formulae is to derive the angular dependence of the fermionic decays of a massive vector boson. For coupling to a left-handed fermion, we have

$$i\mathcal{M} \sim \epsilon^{\mu}(q) \; u^{\dagger}(p)\, \bar{\sigma}_{\mu}\, v(\bar{p})$$

$$\sim \epsilon^{\mu}(q) \; \sqrt{2}\, 2p\, \epsilon_{L}^{\dagger}(p)$$

$$\sim \sqrt{2}\, 2p\, \epsilon^{\mu}(q)\, (0, \cos\theta,\, i,\, -\sin\theta)_{\mu}$$

The form of this matrix element is

$$
\begin{array}{lll}
\text{for} & V_L & (1+\cos\theta) \\
& V_0 & \sqrt{2}\,\sin\theta \\
& V_R & (1-\cos\theta)
\end{array}
$$

Then

$$\frac{d\Gamma}{d\cos\theta}(V \to \bar{e}_L e_R) \sim
\left\{
\begin{array}{ll}
(1+\cos\theta)^2 & L \\
2\sin^2\theta & 0 \\
(1-\cos\theta)^2 & R
\end{array}
\right.$$

At the LHC, the reactions that are of most interest have momentum transfers much larger than 100 GeV. In tbhis regime, the weak interactions bosons W and Z play an important role. In fact, at these energies, we are above the energy scale of electroweak unification, so the W, Z, and photon are all on the same footing. The electroweak theory has order-1 parity violation. Thus, there does not need to be any symmetry between the production of the parity-conjugate L and R states. If we can identify W and Z bosons, in particular, in their leptonic decays where the fermion and antifermion are distinguished, we can use the angular distributions above to identify the W and Z polarizations and obtain additional insight into the dynamics.

It will be very useful to work out the properties of the W and Z. The electroweak boson couplings to quarks and leptons are determined by the covariant derivatives of $SU(2) \times U(1)$. I hope you are very familiar with these:

$$\delta \mathcal{L} = Q e \, A_\mu \, \bar{f} \gamma^\mu f + \frac{g W_\mu}{\sqrt{2}} \bar{f} \gamma^\mu P_L f$$

$$+ \frac{g}{c_w} Z_\mu \, \bar{f} \gamma^\mu Q_z f$$

where

$$Q_z = \left(I^3 - s_w^2 \, Q \right)$$

I will use the abbreviations

$$c_w = \cos \Theta_w \qquad s_w = \sin \Theta_w$$

A partial width of the W to leptons is given by

$$i \mathcal{M} = i \frac{g}{\sqrt{2}} \, \xi_\mu(q) \, v^\dagger \bar{\sigma}^\mu u \cdot i \frac{g}{\sqrt{2}} \sqrt{2} \, 2p \, \xi_\mu(q) \, \xi_L^{*\mu}(p)$$

$$|\mathcal{M}|^2 = g^2 m_w \, |\vec{\xi}_w \cdot \vec{\xi}_p|^2$$

Then

$$\Gamma = \frac{1}{8\pi} g^2 m_w \cdot \frac{1}{3} = \frac{\alpha_w}{12} m_w$$

and the partial widths are the same for all three lepton doublets

9

$$(\nu_e \, e)_L \qquad (\nu_\mu \, \mu)_L \qquad (\nu_\tau \, \tau)_L$$

up to very small mass effects. For the two accessible quark doublets

$$(u\,d)_L \qquad (c\,s)_L$$

the rate of a W decay is multiplied by

$$3\left(1 + \frac{\alpha_s(m_W)}{\pi} + ..\right) \cong 3.1$$

To evaluate these formula and other in this course, it will be good to have a standard set of coupling constants. All Standard Model couplings run according to the renormalization group, so I will canonically quote the values at $Q = m_Z$. You might want to memorize these values:

$$\alpha = \frac{e^2}{4\pi} = \frac{1}{128.}$$

$$\alpha_w = \frac{g^2}{4\pi} = \frac{e^2}{4\pi s_w^2} = \frac{1}{30.}$$

with

$$\alpha_w' = \frac{g'^2}{4\pi} = \frac{e^2}{4\pi c_w^2} = \frac{1}{98.}$$

$$s_w^2 = 0.231$$

The strong interaction coupling is also a weak coupling at high energies because of asymptotic freedom. At LHC energies, it is not so much larger than the electroweak couplings

10

$$\alpha_s = \frac{g_s^2}{4\pi} \approx \frac{1}{8.5}$$

Using the values above, we find for the W boson width

$$\Gamma_w = \frac{\alpha_w m_w}{12} \underbrace{[\ 3\ }_{e\mu\tau} + \underbrace{2(3.1)]}_{uc} \approx 2.1 \text{ GeV}$$

with the branching ratios

$$BR(e\nu) = BR(\mu\nu) = BR(\tau\nu) = 11\%$$

$$BR(u\bar{d}) = BR(c\bar{s}) = 34\%$$

Figures 1-3 show some $e^+e^- \to W^+W^-$ events recorded at LEP, a 200 GeV e^+e^- collider operated at CERN in the 1990's, showing W decays into hadronic and leptonic final states.

We can go through the same analysis to find the properties of the Z. The partial width for a Z decay to left-handed fermions is obtained from the matrix element

$$i\mathcal{M} = \frac{g}{c_w} \varepsilon_Z^\mu u^\dagger \bar{\sigma}_\mu v\ Q_Z$$

Following the same route as for the W, we obtain

$$\Gamma(Z^0 \to f_L \bar{f}_R) = \frac{\alpha_w}{6 c_w^2} m_Z\ Q_Z^2$$

The factors Q_Z are quite different for the various Standard Model species of quarks and leptons. It is useful to make a table; Let S_f and A_f be the combinations of Z charges,

$$e^+ e^- \rightarrow W^+ W^-$$

$$\rightarrow e\, \bar{\nu}\, \mu\, \nu$$
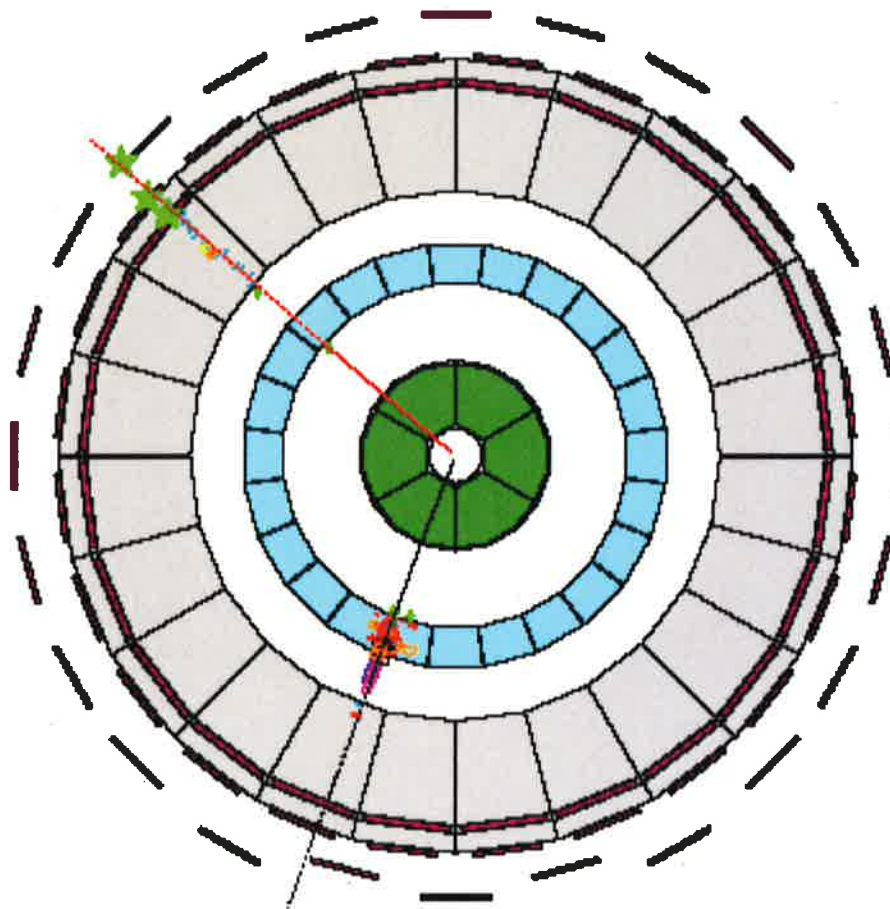
DELPHI

Fig. 1. An $e^+e^- \rightarrow W^+W^- \rightarrow e\nu\,\mu\nu$ event recorded by the DELPHI detector at LEP

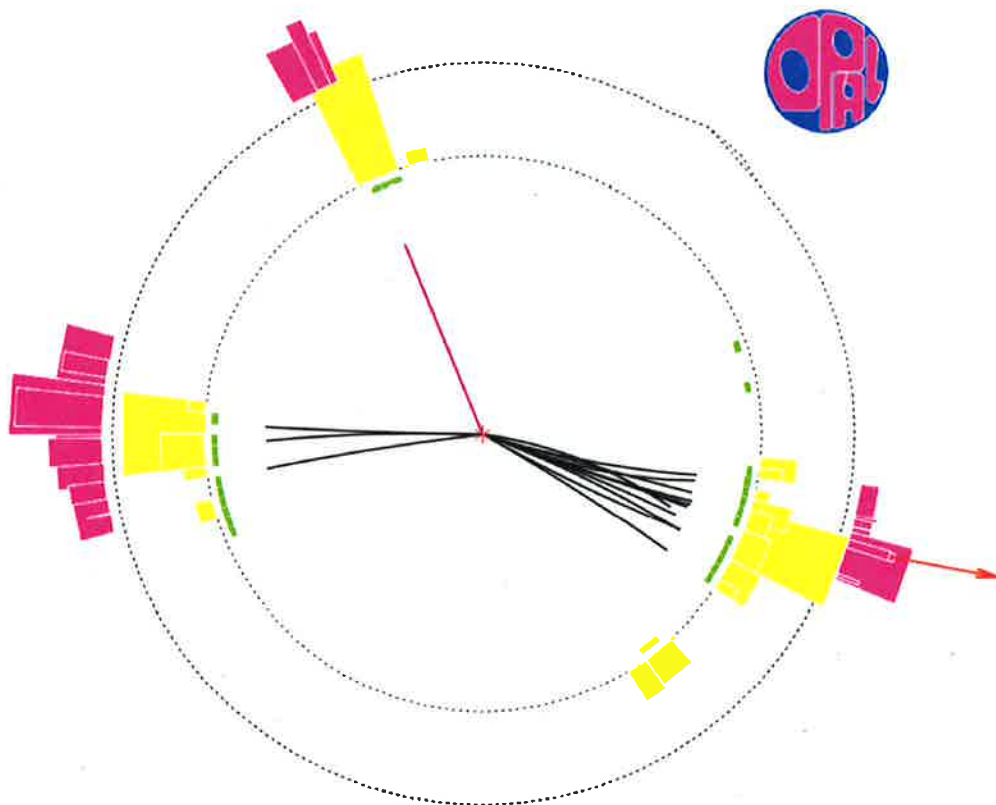$$e^+e^- \rightarrow W^+W^- \rightarrow q\bar{q}\tau\nu$$

Fig. 2   An $e^+e^- \rightarrow W^+W^- \rightarrow q\bar{q}\tau\nu$ event recorded by the OPAL detector at LEP.
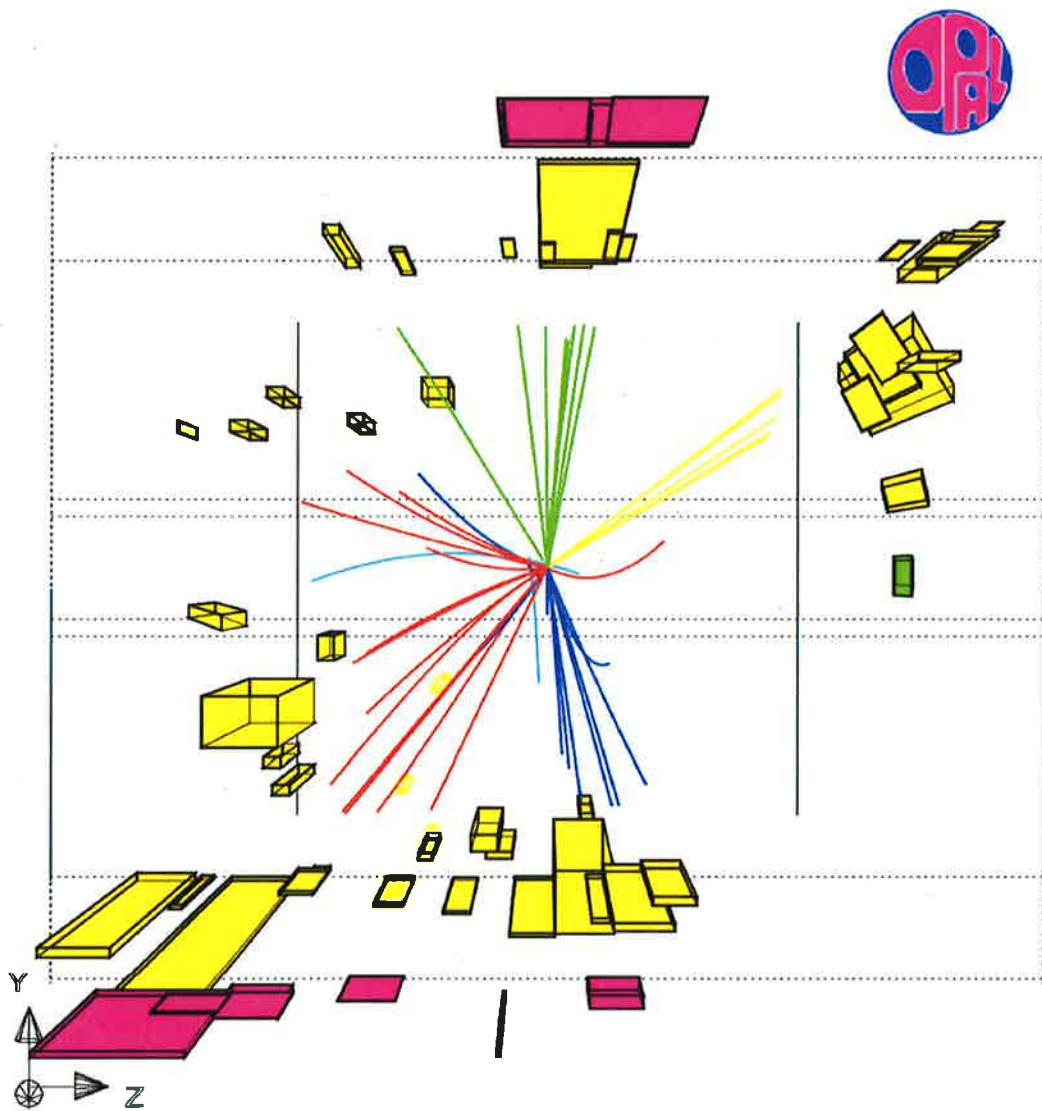
Fig. 3   An $e^+e^- \to W^+W^- \to q\bar{q}\, q\bar{q}$ event recorded by the OPAL detector at LEP.

$$S_f = Q_z^2(L) + Q_z^2(R) \qquad A_f = \frac{Q_z^2(L) - Q_z^2(R)}{Q_z^2(L) + Q_z^2(R)}$$

S_f gives the total rate for Z decay into a given species. A_f gives the asymmetry between left- and right-handed fermions appearing in the decay. Then the Z charges are

species	$Q_z(L)$	$Q_z(R)$	S_f	A_f
ν	$\frac{1}{2}$	$-$	0.25	1
e	$-\frac{1}{2}+s_w^2$	s_w^2	0.126	0.15
u	$\frac{1}{2}-\frac{2}{3}s_w^2$	$-\frac{2}{3}s_w^2$	0.144	0.67
d	$-\frac{1}{2}+\frac{1}{3}s_w^2$	$+\frac{1}{3}s_w^2$	0.185	0.93

The total width of the Z is

$$\Gamma = \frac{\alpha_w m_z}{6 c_w^2}\Big[\ 3\cdot(0.25) \underset{\nu}{} + 3\,(0.126) \underset{e\mu\tau}{}$$

$$+\ 2\,(3.1)(0.144) \underset{u,c}{} + (2.96)(3.1)(0.185)\Big]$$

$$=\ 2.49\ \text{GeV}$$

The small shift in the b coupling to the Z is due to the contribution of diagrams involving the top quark
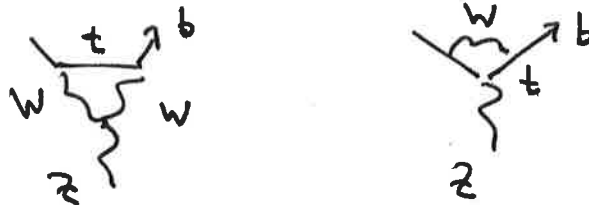
The branching ratios are, then

$$BR(\nu_e \bar{\nu_e}) = 6.7\%$$

$$BR(3\nu\bar{s}) = 20\%$$

$$BR(e^-\bar{e}) = BR(\mu^+\bar{\mu}) = BR(\tau^+\bar{\tau}) = 3.3\%$$

$$BR(u\bar{u}) = 11.9\%$$

$$BR(d\bar{d}) = 15.3\%$$

These branching ratios are very well verified experimentally. In the 1990's, experiments at LEP and at the SLC collider at SLAC produced a large sample of $e^+e^- \to Z$ events and observed the Z decaying at rest. Figures 4-6 show some Z decays recorded by the SLD detector at the SLC, illustrating some of these classes of Z decays.

There is no time in the course for a complete discussion of experimentation in collider physics. But I would like to say a few words about how events are recorded in collider detectors and how to interpret these figures. A schematic plan of one of the LEP detectors is shown in Fig. 7. The e^+e^- collision is arranged to occur in the center of the detector. A high energy collision—after the decay of short-lived particles—produces 6 types of long-lived elementary particles, for which the detector should try to observe as many as possible. These are:

1. electrons

2. photons (mainly from $\pi^0 \to 2\gamma$, but also directly produced)

3. long-lived charged hadrons (π, K, p, ...)

4. long-lived neutral hadrons (n, K^0, Λ^0, ...)

5. muons

6. neutrinos

The detector should be designed to measure the momenta of as many particles over as large a solid angle as possible. It is a challenge, because a detector for one type of particle will interact with all other types and degrade their measurement.

The basic design used to measure particles at colliders was introduced in the Mark I experiment of the 1970's at SLAC, the experiment that also discovered the ψ family of particles, the charmed particles, and the τ lepton. The idea was the construct the detector as a barrel around the interaction point, in such a way that each inner layer minimally compromises the measurements in the outer layers.

The most precise measurements are those of the trajectories of charged particles in a magnetic field. So the interior of the detector is mostly empty space, with a

$e^+e^- \rightarrow Z^0 \rightarrow e^+e^-$

SLD
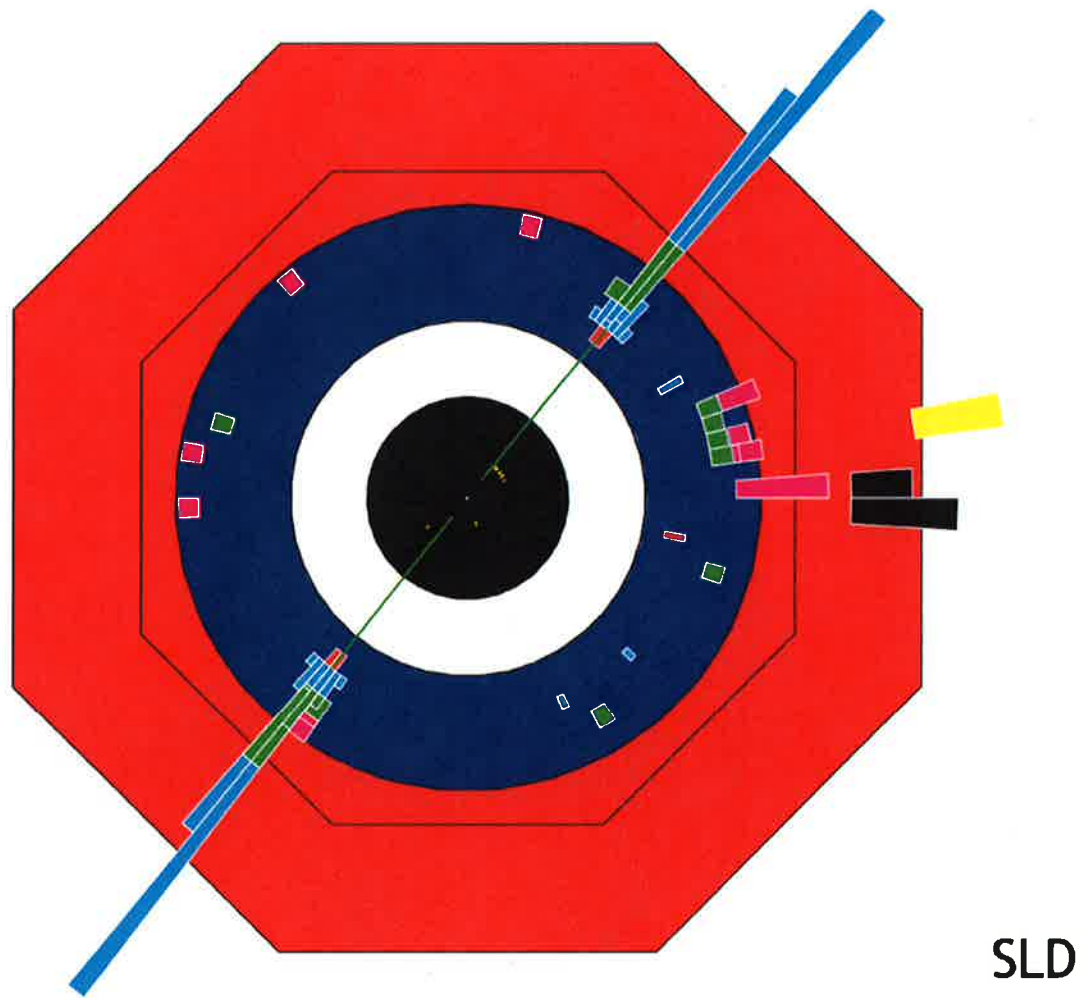
Fig. 4   An $e^+e^- \rightarrow Z^0 \rightarrow e^+e^-$ event recorded
by the   SLD detector at the LHC.
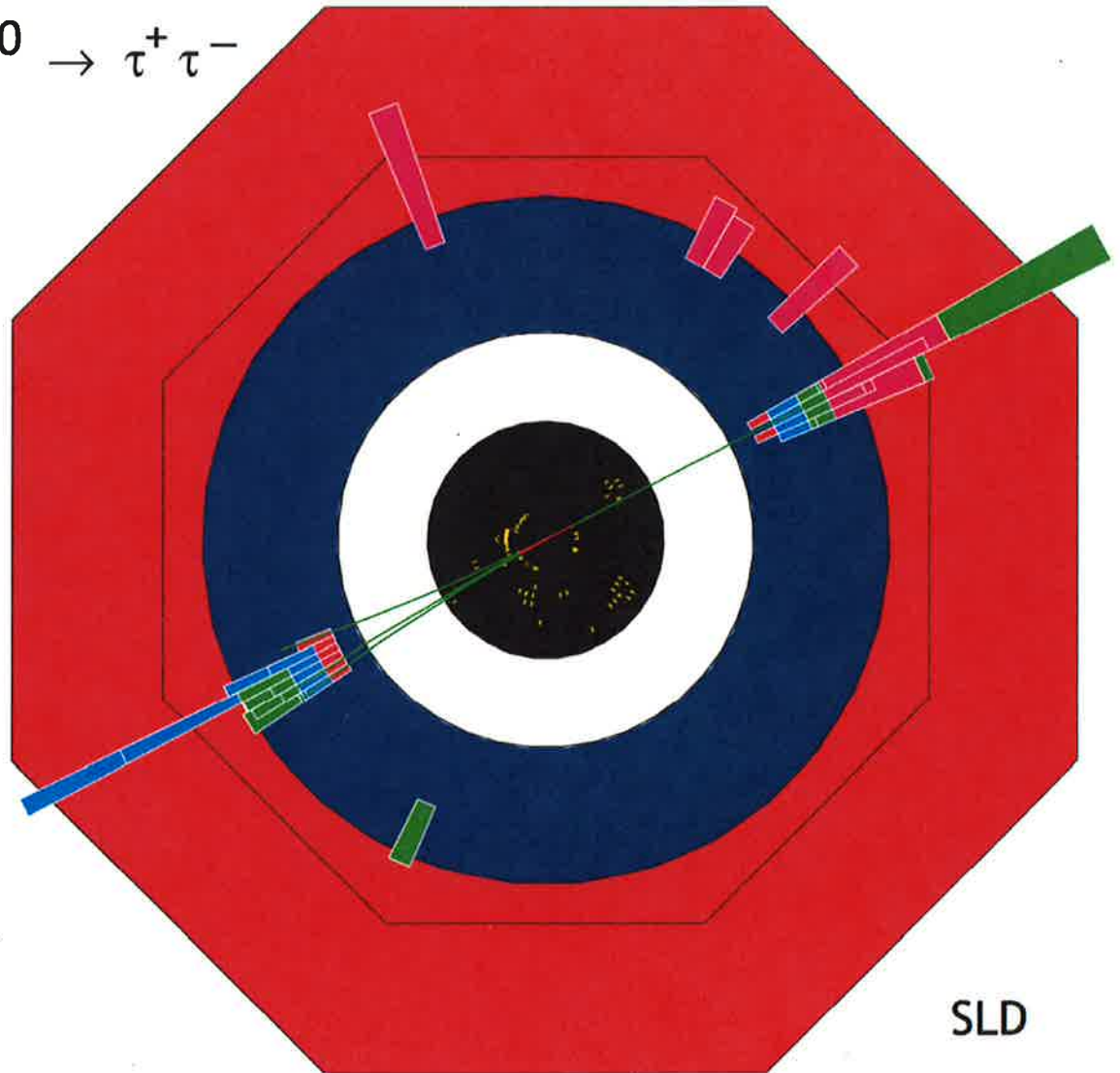
$e^+e^- \rightarrow Z^0 \rightarrow \tau^+\tau^-$
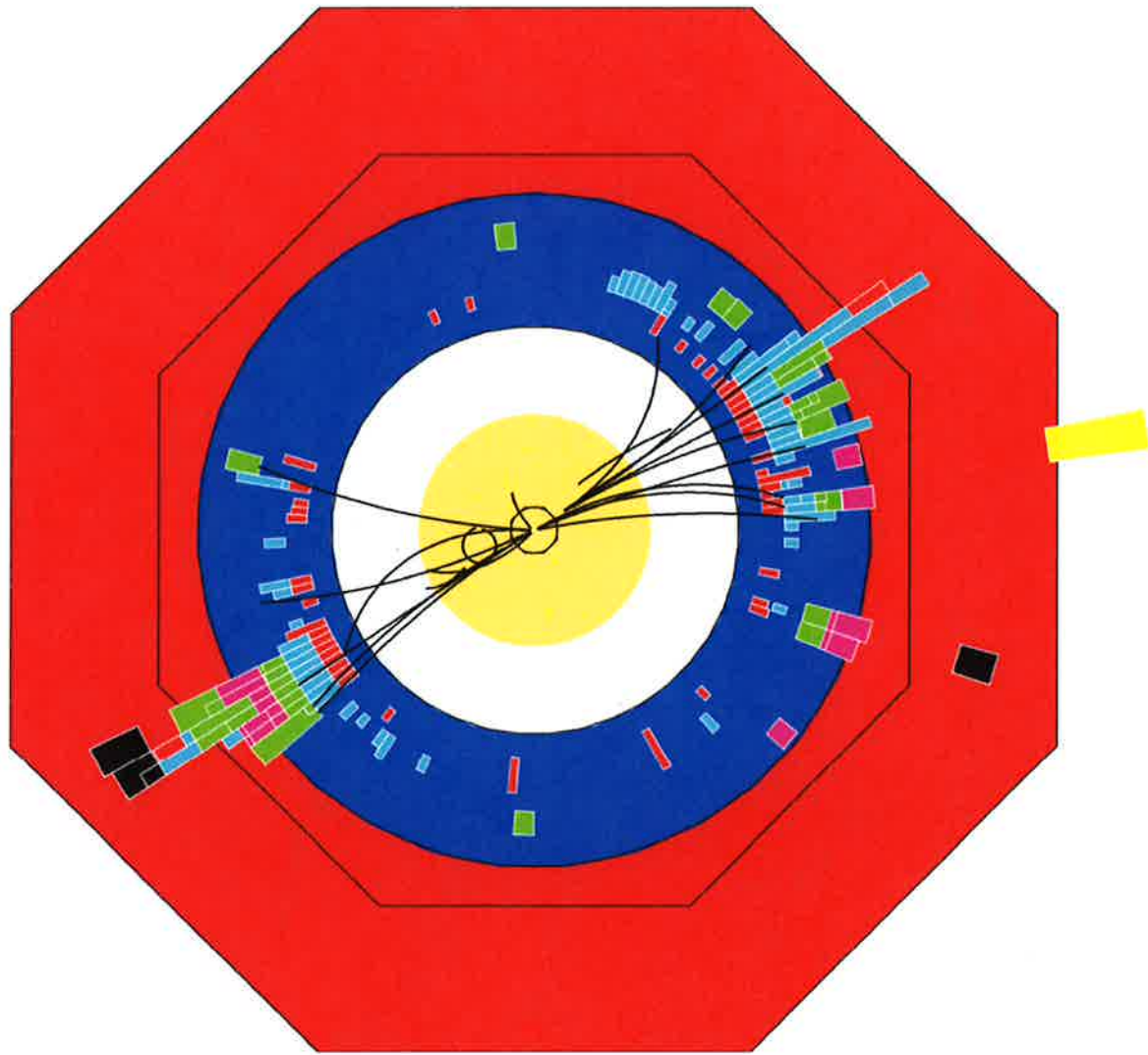

Fig. 5   An $e^+e^- \rightarrow Z^0 \rightarrow \tau^+\tau^-$ event recorded by the SLD detector at the LHC.

SLD

Fig. 6 An $e^+e^- \rightarrow Z^0 \rightarrow q\bar{q}$ event recorded by the SLD detector at the LHC.

Hadron calorimeters and return yoke

Electromagnetic calorimeters

Muon detectors

Jet chamber

Vertex chamber

Microvertex detector

Z chambers

y

θ φ

z x

Forward detector

Silicon tungsten luminometer

Presamplers

Time of flight detector

Solenoid and pressure vessel

OPAL

Fig. 7   Schematic diagram of the OPAL detector at LEP.   From LEP Electroweak Workg Grp, arXiv: hep-ex/0509008   Phys. Repts. 427, 257 (2006),

gas chamber or silicon devices to measured the tracks of charged particles from their ionization. Modern detectors also contain high-precision silicon sensors very close to the interaction point.

The next types of particles to measure are electrons and photons.. Above an energy of about 10 MeV, electrons radiate hard photons as they pass through matter, and photons convert to electron-positron pairs. This gives rise to an electromagnetic showers in which the number of electrons, positrons, and photons multiplies.

Measurement of the ionization within the shower gives the total energy of the electron or positron that initiated it. A detector built on this principle is called an electromagnetic calorimenter; The characteristic length for multiplication in a shower is called the radiation length. A high-Z material such as Pb has a radiation length of about 0.5 cm; then a 17-cm thickness corresponds to 30 radiation lengths, enough to contain an electromagnetic shower. The same thickness of Pb corresponds to about 1 nuclear interaction length.

Ourside the electromagnetic calorimeter, one can switch to a cheaper material such as Fe and to coarser segmentation. In a few hundred cm of Fe, an initial π^+ or n will create a hadronic shower, giving a basis for hadronic total energy measurement. Finally, any charged particle that can go through the hadron calorimeter is probably a muon, and one can put ionization detectors on the outside of the detector to identify these particles and determine their trajectories. Neutrinos – and other possible neutral, weakly-interacting particles – are invisible to collider detectors.

Some typical performance estimates, for guidance only are:

$$\text{tracking}: \qquad \frac{\Delta p_T}{p_T} \sim 3\% \left(\frac{p_T}{100 \; \text{GeV}} \right)$$

$$\text{EM calorimetry}: \qquad \frac{\Delta E}{E} \sim \frac{10\%}{\sqrt{E/\text{GeV}}}$$

$$\text{hadron calorimetry}: \qquad \frac{\Delta E}{E} \sim 50\% / \sqrt{E/\text{GeV}}$$

The important information to take away from these equations is the way that the measurement accuracy depends on the value. In particular, calorimetry becomes

14

more accurate for large energy deposition. momentum measurement loses accuracy for very high-energy tracks, and even the sign of a multi-TeV muon can be uncertain.

There is an important complication in this design: The detector must also contain a solenoidal magnet to producee the magnetic field needed to bend the trajectories of charged particles. A superconducting magnet with its cryostat contributes about 2 radiation lengths of material. So, one has a choice whether to put the electromagnetic calorimeter outside the coil and have its measurement compromised or to put the calorimeter inside the coil and pay for a larger and more difficult magnet. At the LHC, ATLAS and CMS made opposite choices here.

With the detector laid out in this way, you see the main components reflected in the event displays. Charged particle tracks are shown explicitly in the interior, and energy deposition in the calorimeter layers is also indicated. Then, for example, a track leading to a large electromagnetic deposition signals an electron.

The way the detectors see quarks needs to be qualified a bit. In the fraction of Z decay events corresponding to $Z \to q\bar{q}$, what we actually see is a collimated stream of strongly interaction particles, mainly pions. In typical events, two such streams are emitted back-to-back. These streams are called "jets". In collider physics, jets are the observable manifestation of quarks and gluons emitted in the high-energy reactions. Jets are not hard to recognize in the pictures but are rather subtle to describe quantitatively. I will discuss the formation and structure of jets in lecture 3 of this series. In $Z \to q\bar{q}$ decays, we have some evidence that the jets represent quarks in the fact that the angular distribution of the jet axes follows the predicted dependence

$$\frac{d\sigma}{d\cos\theta} \sim (1 + \cos^2\theta)$$

The data from the ALEPH detector at LEP is shown in Fig. 8.

It is important to note that the charm and bottom quarks are short-lived, so the presence of these quarks must be inferred from their decay products. The bottom quark has a longer lifetime of 1.5 ps, corresponding to a $c\tau$ of 0.5 mm, typically enhanced by a Lorentz boost. Decay vertices a few mm from the collision point can be identified by precision silicon tracking detectors, giving a way to tag the production of b quarks and, to some extent c quarks also.

The τ lepton shows up in detectors in a wide variety of ways. The τ decays to a ν_τ, which may be accompanied by either hadrons or leptons. The dominant branching fractions of the τ are
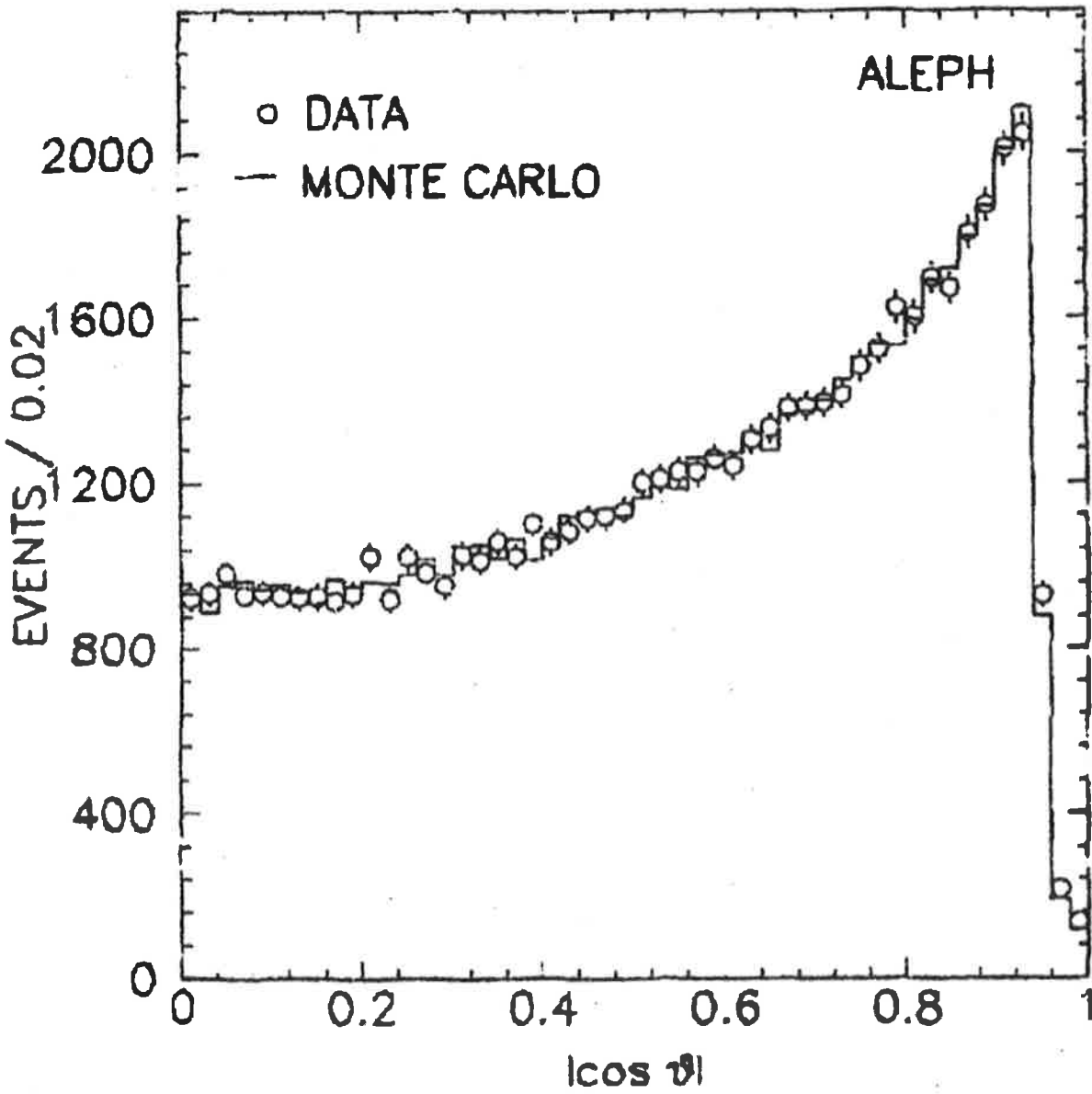
Fig. 8   Angular distribution of jets in
$e^+e^- \rightarrow Z^0 \rightarrow q\bar{q}$, from   D. Decamp et al.
Z Phys. C   48, 365 (1990)

$$\tau^- \longrightarrow \begin{array}{ll} \nu_\tau\, e^-\bar{\nu}_e & 17.5\% \\ \nu_\tau\, \mu^-\bar{\nu}_\mu & 17.5\% \\ \nu_\tau\, \pi^- & 11\% \\ \nu_\tau\, \rho^-\,(\pi^-\pi^0) & 26\% \\ \nu_\tau\, a_1^-\,(3\pi) & 19\% \end{array} \left.\begin{array}{l} \\ \\ \\ \\ \\ \end{array}\right\} 9\,\%$$

So events with τ pairs fall into a number of different categories — 2 lepton, 1 lepton plus 1 hadron, etc. In e^+e^- collisions, the most characteristic topology for the τ^+ is 1 pion plus 3 pions.

Using these techniques, the LEP and SLC detectors made it possible to separate the various Z decays and measure their branching fractions. Some notable results are:

		from above	SM w. $\theta(\alpha)$	expt.
$R_\ell = \dfrac{\Gamma(Z \to \text{hadrons})}{\Gamma(Z \to \mu^+\mu^-)}$		20.6	20.739(18)	20.767(25)
$R_b = \dfrac{\Gamma(Z \to b\bar{b})}{\Gamma(Z \to \text{hadrons})}$		0.213	0.21562(13)	0.21629(66)
$\Gamma_{Z,\text{tot}}\,(\text{GeV})$		2.49	2.4965(15)	2.4952(23)

The quantities A_f in the table above, giving the left/right polarization asymmetries, are also observable. These cover a large range, from 15% for leptons to 93% for d quarks. These predictions have also been tested using τ decays at LEP and experiments with polarized electron beams at the SLC. Some results are

	from above	SM in $\theta(\alpha)$	expl-
A_e	0.15	0.1460(11)	0.1513(21)
A_τ	0.15	0.1460(11)	0.1463(33)
A_b	0.93	0.935(1)	0.923(20)

So, the couplings of the Z and, by extension, the structure of the electroweak interactions in the Standard Model, is very well confirmed experimentally.

The parity asymmetries of the weak interactions show up as forward-backward asymmetries in $e^+e^- \to f\bar{f}$ even when we average and sum over polarizations. The differential cross section for $e^+e^- \to f\bar{f}$, taking into account γ-Z interforence, is

$$\frac{d\sigma}{d\cos\theta} = \frac{1}{4}\left[\frac{d\sigma}{d\cos\theta}(\bar{e}_L e_R^+ \to f_L \bar{f}_R) + \frac{d\sigma}{d\cos\theta}(\bar{e}_R e_L^+ \to f_R \bar{f}_L)\right.$$

$$\left. + \frac{d\sigma}{d\cos\theta}(\bar{e}_L e_R^+ \to f_R \bar{f}_L) + \frac{d\sigma}{d\cos\theta}(\bar{e}_R e_L^+ \to f_L \bar{f}_R)\right]$$

$$= \frac{\pi\alpha^2}{8s}\left[(1+\cos\theta)^2\left|-Q + \frac{(-\frac{1}{2}+s_w^2)(I^3-Qs_w^2)}{s_w^2 c_w^2(1-m_Z^2/s)}\right|^2 + \left|-Q + \frac{s_w^2(-Qs_w^2)}{c_w^2 s_w^2(1-m_Z^2/s)}\right|^2\right.$$

$$\left. + (1-\cos\theta)^2\left|-Q + \frac{(-\frac{1}{2}+s_w^2)(-Qs_w^2)}{s_w^2 c_w^2(1-m_Z^2/s)}\right|^2 + \left|-Q\frac{s_w^2(I^3-Qs_w^2)}{c_w^2 s_w^2(1-m_Z^2/s)}\right|^2\right]$$

You can see the constructive interference in the first line of the result and the destructive interference in the second line, so there is a forward-backward asymmetry that becomes of order 1 for $s > m_Z^2$. The total cross section is shown in Fig. 9, along with measurements at LEP, SLC, and lower energy colliders. This has a prominent resonance at the Z, with a discontinuity in the normalization on the two sides of the resonance resulting from the interference.

It is quite interesting to take the limit $s \gg m_Z^2$. Then the first square in the result above becomes

$$e^2\left(-Q + \frac{(-\frac{1}{2}+s_w^2)(I^3-Qs_w^2)}{s_w^2 c_w^2}\right) = e^2\left(-(I^3+Y) + \frac{(\frac{1}{2}+s_w^2)(I^3 c_w^2 - Y s_w^2)}{c_w^2 s_w^2}\right)$$

$$= e^2\left(I^3[-1-\frac{1}{2s_w^2}+1]\right) + Y\left(-1 + \frac{1}{2}\frac{1}{c_w^2} - \frac{s_w^2}{c_w^2}\right)$$

$$= e^2\left(I_e^3 \frac{1}{s_w^2} I^3 + Y_e \frac{e^2}{c_w^2} Y\right)$$

or, finally,

$$= I_e^3 \frac{e^2}{s_w^2} I^3 + Y_e \frac{e^2}{c_w^2} Y$$

The answer is what we would expect for an unbroken $SU(2) \times U(1)$ model
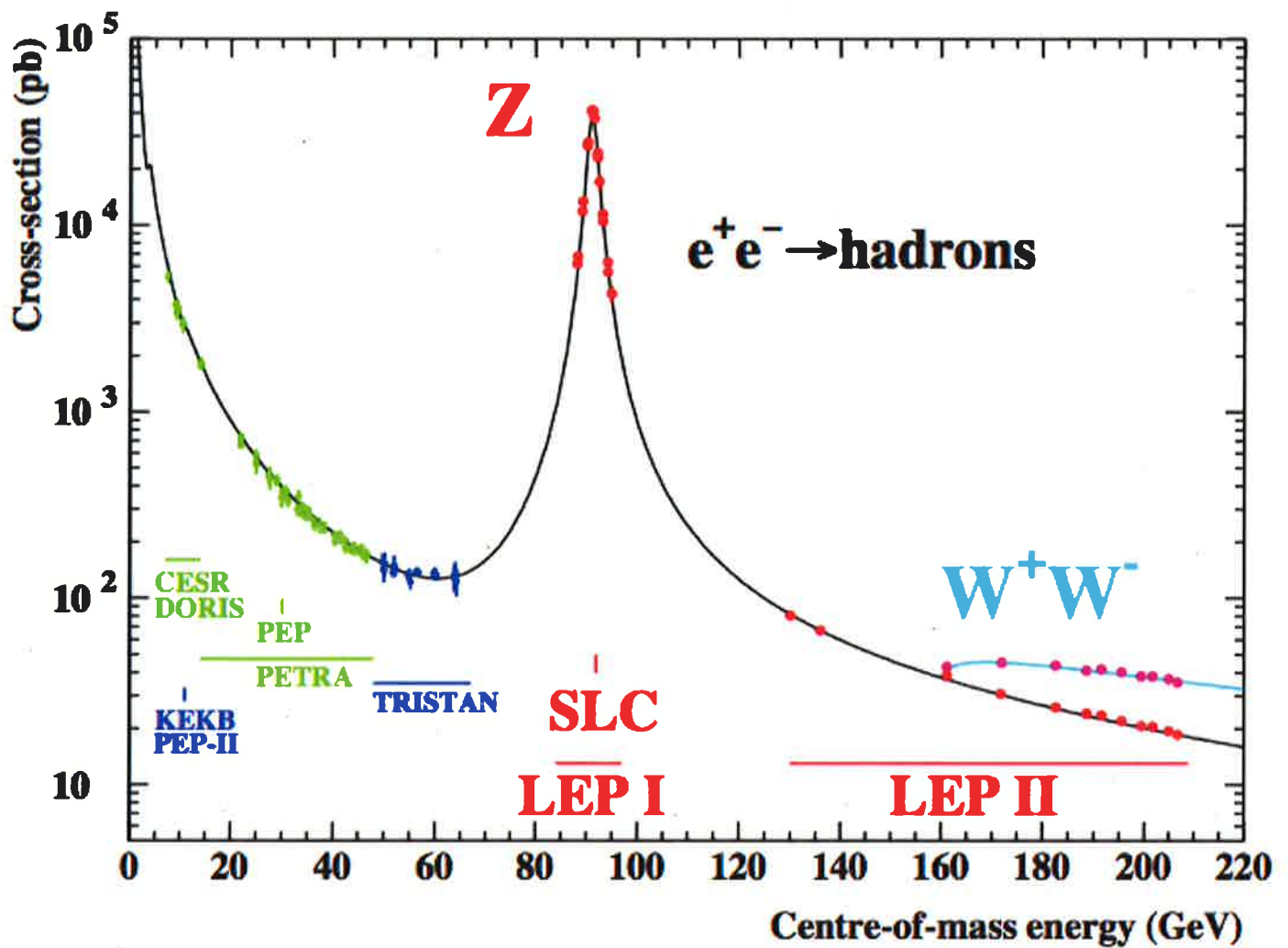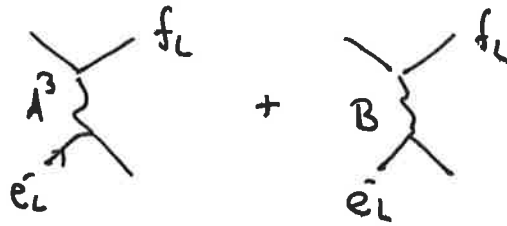
17

Fig. 9 Total cross sections in e⁺e⁻ annihilation, from LEP Electroweak Working Group, arXiv: hep-ex/0509008 Phys. Repts. 427 257 (2006).

You can check that this works for the other contributions as well. This limit of high energy, with manifest $SU(2) \times U(1)$ symmetry, is very useful to understand many aspects of the physics at the LHC.